Journal of Russian Laser Research, Volume 19, Number 2, 1998

MONOCHROMATIC X-RAY SOURCES BASED ON EMITTERS CONTROLLED BY LASER RADIATION

Yu. V. Korobkin, V. B. Rozanov, A. S. Shikanov, and G. A. Vergunova

P. N. Lebedev Physical Institute, Russian Academy of Sciences, Leninskii Pr. 53, Moscow 117924, Russia

Abstract

The results of study of frequency-tuned monochromatic x-ray source are reported. The source was developed on the basis of a vacuum diode with a laser-plasma cathode. The source proposed is particularly promising, if the range of x-ray energy higher than 5 keV is of interest. The source features a spectral brightness higher than 10^{19} photons/(cm^2·s·sr·keV) and an x-ray pulse duration no larger than 10^{-8} s. An electromagnetic model of such a cathode is proposed and evaluated in order to assess the feasibility of an x-ray source with a laser-plasma cathode of higher performance. The possibility of using a ferroelectric electron emitter is discussed.

1. Introduction

Time-synchronized pulsed x-ray radiation is useful studying the evolution of nonsteady microobjects (including laser plasmas), which feature large density and refractive-index gradients. In this paper, we report a design of a source of such radiation on the basis of a vacuum diode provided with laser-plasma or ferroelectric cathodes; both of these cathodes, according to our estimates, have a number of advantages over the x-ray source types that are regarded as the most promising at present and include an auxiliary target irradiated by a diagnostic laser.

It is anticipated that the new source will have spectral brightness higher than 10^{19} photons/(cm^2·s·sr·keV) and a pulse duration shorter than 10^{-8} s.

2. X-Ray Radiation Sources and Probing Techniques

X-ray probing of dense plasma was first accomplished at the Rutherford Ampleton Laboratory [1, 2]. This technique was further developed in France [3], Japan [4], and the USA [5, 6]. It was demonstrated that the plasma of an auxiliary target irradiated by a diagnostic laser pulse is the most convenient source of probing x-ray radiation with given parameters (such as spectrum, brightness, pulse duration, and synchronization). Since the parameters of the formed plasma are known functions of the laser flux and target composition, such a source largely meets experimental requirements.

The requirements imposed on various schemes of x-ray probing stem from the fact that the intensity of probing radiation beyond the microobject must be sufficiently high to be detected with allowance for the detector sensitivity and the background radiation. This condition can be met if the wavelength of probing radiation is much shorter than the critical one. In particular, in the case of a dense nonuniform plasma with electron density $n_0 \sim 10^{22}$ cm^{-3}, it is required that $\lambda < 0.3$ nm. Furthermore, owing to the dependence of mass absorption coefficient μ on wavelength ($\mu \propto \lambda^3$), an unambiguous interpretation of results is possible only if the sources are monochromatic and have brightness exceeding the intensity of the microobject's intrinsic emission.

In this respect, the laser plasma formed at auxiliary targets made of elements with large atomic number [1–6] seems to be the most appropriate source of x-ray radiation. The main drawbacks of such a source consist

Translated from Preprint No. 27 of the P. N. Lebedev Physical Institute (1995).

 1071-2836/98/1902-0134$20.00

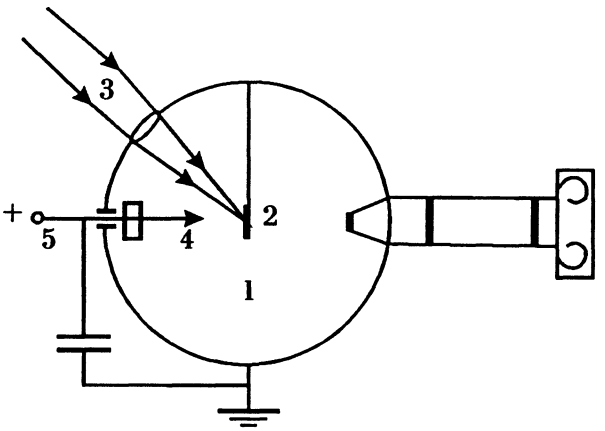

Fig. 1. Schematic layout of experimental setup: 1) vacuum chamber, 2) target, 3) laser beam, 4) titanium anode, and 5) high-voltage power supply.

in (i) the necessity of employing a high-power diagnostic laser (because the intensity of laser-plasma x-ray radiation in the resonance K lines decreases drastically with an energy of quanta exceeding 4 keV) [7, 8] and (ii) the requirement for monochromatization of the radiation.

3. Development and Study of X-Ray Sources Based on Laser-Plasma Cathodes

For a probing source, we suggest an x-ray tube, which is mounted in a vacuum chamber and emits the K lines of the cathode material bombarded by accelerated electrons of the laser plasma [9]. A schematic diagram of experimental setup is shown in Fig. 1. Vacuum chamber 1 accommodates the target 2 made of aluminum foil ≈ 100 μm thick. The target is exposed to nanosecond or picosecond pulses 3 of Nd-laser radiation (or its harmonic). The laser beam is focused at the target to a spot of about 50 μm in diameter with the use of an optical system.

The electric circuit of the x-ray source involves the grounded target 2, which serves as a cathode, and an anode 4 kept under positive dc voltage of (5–25) kV derived from a high-voltage power supply 5.

Electrons emitted from the plasma formed at the cathode under the effect of laser-induced heating are accelerated by an electric field in the direction of the cone-shaped anode and initiate x-ray emission concentrated in the characteristic K lines of the anode material. In this case, the plasma acting as an electron emitter is formed under laser irradiation of the target irrespective of the applied accelerating voltage [10].

It is known that the highest yield of characteristic x-ray emission is realized for an electron energy 2.7–3 times higher than the energy of the corresponding transition [11]. In particular, if the optimum accelerating voltage is used, the intensity of continuous bremsstrahlung is reduced markedly and, as a result, the radiation becomes more monochromatic [12]. On the basis of such a system involving a Nd laser with energy of 0.2 J and pulse duration of 8 ns, a laser-plasma cathode, and a titanium anode, we developed a source of characteristic x-ray radiation concentrated in the K lines of Ti, which features a pulse duration less than 20 ns and spectral brightness of 10^{19} photons/(cm^2·s·sr·keV). Figure 2 illustrates dependences of the current-signal amplitude and overall x-ray yield on the anode voltage. Dependences of the pulse duration and overall x-ray yield on the anode–cathode separation are shown in Fig. 3.

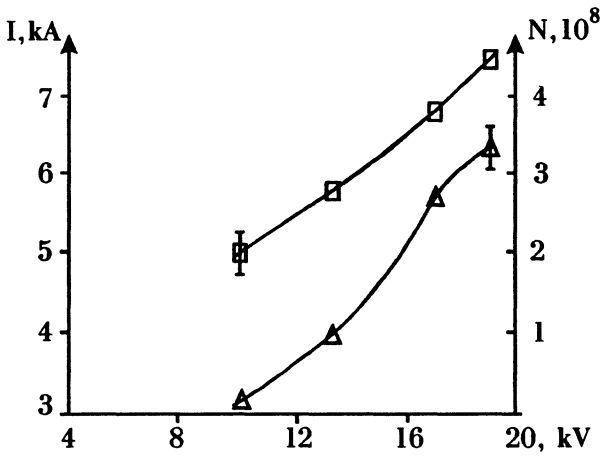

Fig. 2. The amplitude of current signal and total yield of x-ray radiation in relation to the anode voltage.

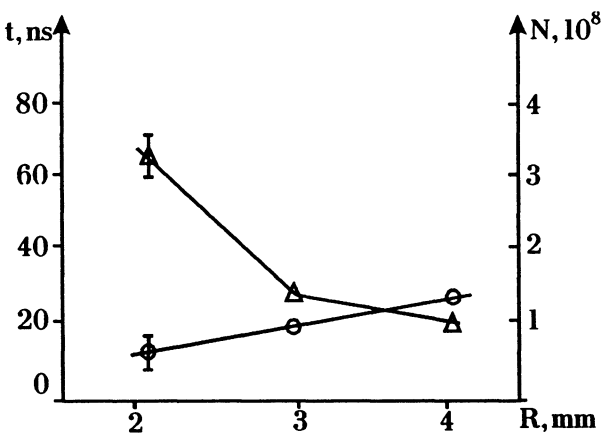

Fig. 3. The duration and total yield of x-ray radiation in relation to the anode–cathode separation.

Let us consider the advantages of the proposed method for producing the probing x-ray radiation as compared to other methods:

(i) the suggested way of forming the probing beam does not require an additional means for monochromatization of x-ray radiation;

(ii) it is easy to accomplish a point-source operation if a microtip is used as an anode;

(iii) as follows from theoretical estimations, using other materials for the anode or increasing the energy and reducing the pulse duration of laser radiation, we can enhance the spectral brightness of the source by several orders of magnitude;

(iv) the proposed source is especially promising if the aim is to advance into the region of hard x-rays (with energy higher than 5 keV) because both the energy and the degree of monochromaticity of electrons are governed by the applied external field and the anode material;

(v) in the case under consideration, the energy of the external source is used; i.e., the laser plasma serves only as an electron emitter, which makes it possible to use lasers of comparatively low power for forming the

plasma.

4. Scale Dependences for a Laser-Plasma Cathode

In order to assess the feasibility of an x-ray source provided with a large-size laser-plasma cathode, we consider the physical model of such a cathode (Fig. 1).

The design of the x-ray source under consideration is promising due to the following features:

(I) the volume and existence time of the plasma source of electrons can be controlled by the laser beam;

(II) the choice of a tip-shaped anode can provide spatial localization of the x-ray source;

(III) the applied external voltage ensures high energy and monochromaticity of electrons and also their additional focusing;

(IV) the energy of the external source (not that of the laser) is used;

(V) the appropriate choice of anode material and applied voltage determines the energy of x-ray quanta.

In what follows, we discuss or formulate the physical problems that arise.

4.1. The Laser-Plasma Parameters

The characteristic temperature of the plasma (in the region of critical density) formed as a result of exposing a plane target to laser radiation can be assessed from the following formula:

$$T = 4 \cdot 10^3 \left(\frac{q}{10^{14}}\right)^{2/3} \left(\frac{1}{\lambda}\right)^{4/3} \text{[eV]}. \tag{1}$$

Here, q is the laser-radiation flux density (in W/cm^2) at the target and λ is the laser-radiation wavelength (in μm).

Under experimental conditions [9] when $q = 10^{11}$ W/cm^2, $\lambda = 1$ μm, and $E_L = 0.2$ J (henceforth, condition 1), the plasma temperature amounts to $\sim$40 eV. If $q = 2 \cdot 10^{14}$ W/cm^2, $\lambda = 0.53$ μm, and $E_L = 3$ kJ (henceforth, condition 2), the temperature T amounts to about (0.5–1) keV. The total number N of particles in the plasma is given by

$$N = \frac{E_L(\gamma - 1)}{2(1 + Z)kT}, \tag{2}$$

where E_L is the laser-radiation energy, γ is an adiabatic exponent equal to 1.3–1.4, k is the Boltzmann constant, T is the absolute temperature, the factor 1/2 accounts for kinetic energy of the plasma, and Z is the degree of ionization.

In the case $Z = 3 - 4$, the total number of electrons in the plasma is $3 \cdot 10^{15}$. Under condition 2, the total number of electrons can approach 10^{19} with degree of ionization $Z = 20 - 25$.

4.2. An Analysis of Experiments Performed under Condition 1

In [9], $6 \cdot 10^8$ photons with an energy of 4.5 keV were detected. With the quantum efficiency of the anode equal to about 0.1, the number of accelerated electrons striking the anode can reach $6 \cdot 10^9$. This is well below the number of electrons 10^{13} of the plasma cloud, which can fall within the solid angle that corresponds to an anode diameter of 0.3 mm and a cathode–anode separation of 2 mm. On the other hand, the measured current pulse that has an amplitude of 8 kA and a duration of about 20 ns transports the charge between anode and cathode, which amounts to about $3 \cdot 10^{15}$ electrons, i.e., to the total number of electrons in the cloud. This pulse carries an energy $E = IU\tau = 2.7$ J, which is more than ten times higher than the laser-pulse energy. It is noteworthy that in [10] the duration of the current pulse coincides with the plasma-particle transit time

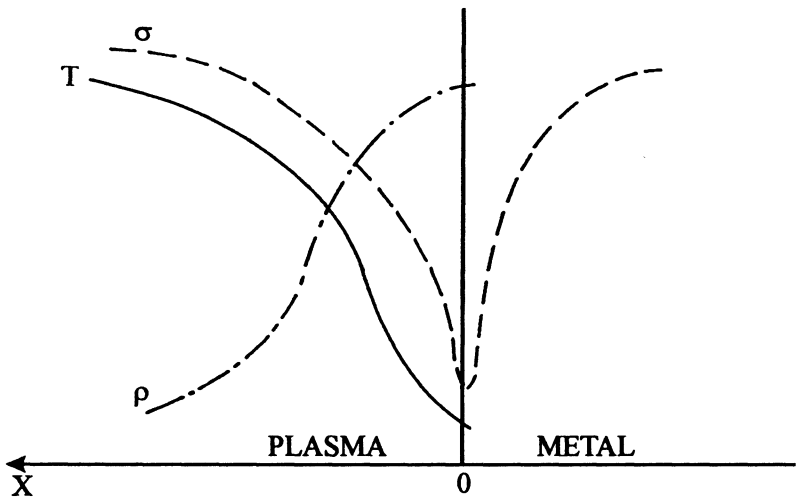

Fig. 4. Illustrative dependences of electrical conductivity, temperature T, and density ρ on the distance in the vicinity of the ablation front.

(equal to about 20 ns) for the cathode–anode gap and, consequently, the current pulse is related not only to the acceleration of a fraction of the electrons, but to the hydrodynamic expansion of plasma as well.

4.3. Charge-Related Constraints

If the voltage U is applied to a spherical cloud of plasma, the charge of the total number of electrons able to leave the cloud owing to the applied voltage is equal to $Q = UR$, where R is the cloud diameter. Later on, the Coulomb forces will impede the flight of electrons from the cloud. For $R = 1$ mm (half of the anode–cathode separation) and $U = 17$ kV, the charge $Q = 5$ (in CGSE units), which is equivalent to 10^{10} electrons. This estimate is verified by measurement of the number of hard x-ray quanta (and, consequently, the number of accelerated electrons, see Sec. 3.2); however, it is appreciably smaller than the number of electrons in the measured current pulse. Certain (yet insignificant) corrections can be related to recombination processes, which occur when the plasma expands. It follows from the relationship

$$dQ = U\,dR = Uv\,dt,$$

where v is the plasma-scatter velocity and dQ is the change of charge of accelerated electrons, that the x-ray pulse can replicate the plasma-expansion pulse.

Based on the analysis performed, we can suggest a model of the plasma cathode operating under conditions 1: a fraction of the accelerated electrons ($\sim 10^{-5}$) produces the x-ray quanta, while the majority of electrons contribute to the current pulse.

4.4. Possible Ways of Overcoming the Charge Constraints

If the cathode is made of a rather large metal plate, it is possible to compensate for the charge carried away by accelerated electrons and considerably increase the proportion of these electrons. The electrical conductivity of metals amounts to 10^{17} s^{-1}, while the electrical conductivity of a plasma $\sigma = 10^{14} T^{3/2}$ s^{-1} (T is expressed in electron volts) and with T =0.1–1 eV is close to the electrical conductivity of metals. Under experimental condition 1, the current density at the anode ($d = 0.1$ mm) is $j = 8 \cdot 10^7$ A/cm^2. Such a

current density can be attained (in accordance with the relationship $j = \sigma E$) for fields E amounting to 300–400 V/cm. This is feasible basically; however, an impediment to realization of this approach will be the region of low electrical conductivity in the vicinity of the ablation front (Fig. 4) where the temperature amounts to several electron volts, metallic conductivity does not yet exist, and there is yet no plasma conductivity.

Other possibilities are related to ionization of residual gas of low density around the cathode and to compensation of the charge of electrons due to electrical conductivity of the surrounding gas.

5. An Analysis of Parameters of Plasma and Laser-Plasma Cathode for a 3-kJ Laser Source

5.1. Formulation of the Problem

In order to analyze the parameters of the plasma and the feasible parameters of a laser-plasma cathode with a laser source energy of 3 kJ, we performed calculations based on the DIANA-NG code. This program is written in the one-dimensional approximation with allowance for a single-liquid two-temperature plasma hydrodynamics, emission from plasma, and radiation transport to a many-group approximation. In this program, allowance is also made for transport and absorption of laser radiation, electronic and ionic thermal conductivities, actual equations of state, exchange of energy between electronic and ionic components, and data on spectral coefficients of absorption and emission of radiation including the procedure of averaging over the groups. A number of other processes are also taken into account in the program.

It follows from our experience in solving one- and two-dimensional problems that calculations in the case of a two-dimensional problem with the flare-type geometry and the given size of focal spot is approximately equivalent to calculations within the framework of a one-dimensional spherical approximation if the actual focal-spot diameter is larger than the radius (but smaller than the diameter) of the sphere used in the one-dimensional calculation with the laser-radiation flux at the sphere surface corresponding to the actual flux at the focal-spot surface. With account taken of this reasoning, we evaluated the processes occurring when a copper spherical shell 750 μm in diameter is exposed to laser radiation with a wavelength $\lambda = 0.53$ μm. The laser radiation flux was represented by a pulse of equilateral-triangle shape, overall duration 3 ns, and peak power density $q_{\max} = 2.5 \cdot 10^{14}$ W/cm^2. For the parameters specified and the actual flare geometry, the laser-radiation energy is given by

$$E_L = \frac{\pi}{4} d^2 \frac{q_{\max}}{2} \tau_{\text{pulse}} = 1.6 \text{ kJ}, \tag{3}$$

where d is the flare diameter.

The thickness of the copper shell is equal to 20 μm; variation of this thickness only slightly affects the plasma parameters. Copper was chosen as a plasma-source material because this element is often used in experiments with rather high atomic numbers. Figures 5 and 6 illustrate the spectral absorption coefficients for copper ($T = 1$ keV and $\rho = 10^{-3}$ g/cm^3 and 3.16 g/cm^3).

5.2. Results of Calculations

Figure 7a illustrates the distributions of density, electron temperature, and plasma-motion velocity for $t = 1.5$ ns (the flux peak) in relation to the number of calculational cells (total number of cells $N = 64$); the same dependences are shown in Fig. 7b on a more expanded scale. In Fig. 7c, the same quantities are plotted as functions of the radius. The relation between the cell number and the radius is illustrated in Fig. 7d for the case $t = 1.5$ ns. Figures 8a and 8b show the radiation flux I_ν as a function of the energy of quanta at the plasma boundary ($N = 64$) and at the boundary between the zone heated due to electronic thermal conductance and the radiant-heating wave front ($N = 62$). Figures 9a and 9b illustrate the distributions

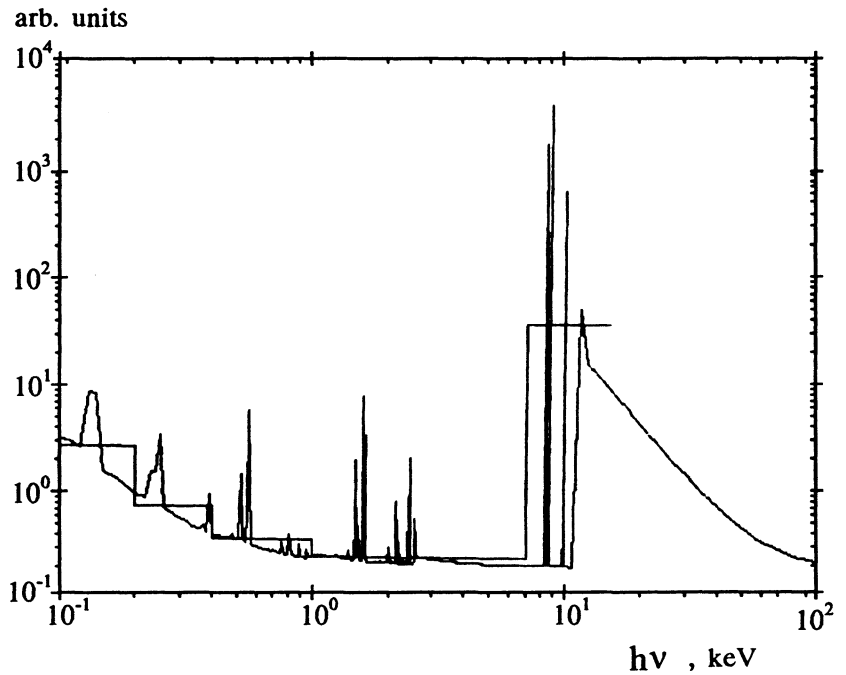

Fig. 5. Spectral absorption coefficients for Cu ($T = 1$ keV and $\rho = 10^3$ g/cm^3).

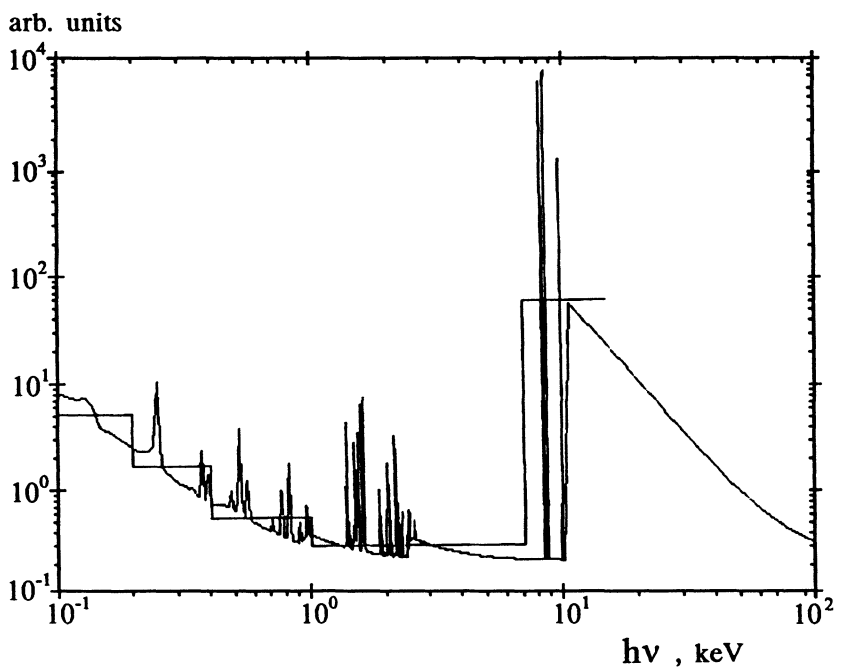

Fig. 6. Spectral absorption coefficients for Cu ($T = 1$ keV and $\rho = 3.16 \cdot 10^3$ g/cm^3).

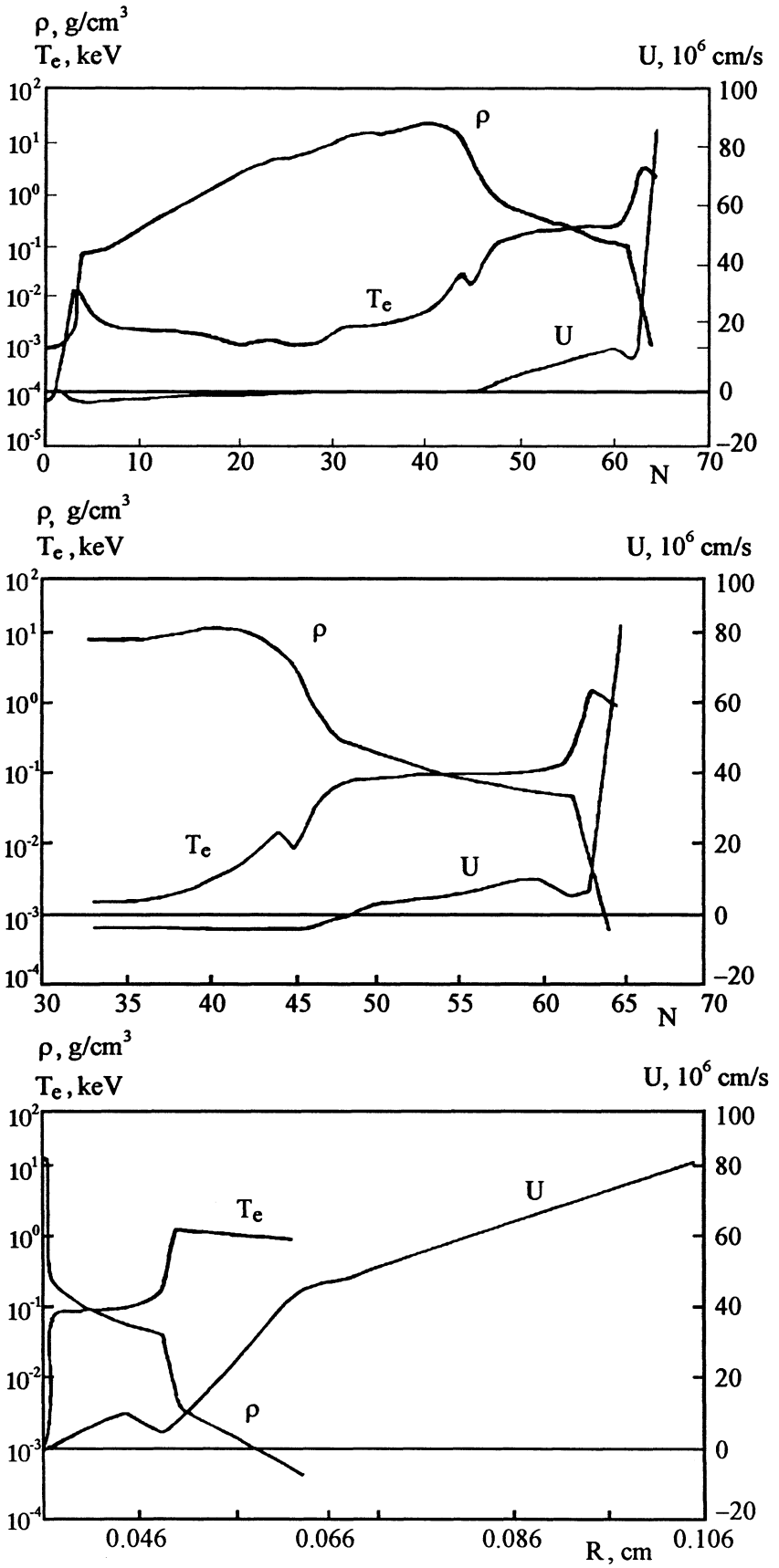
ρ, g/cm³
Te, keV
U, 10⁶ cm/s
ρ
Te
U
N
ρ, g/cm³
Te, keV
U, 10⁶ cm/s
ρ
Te
U
N
ρ, g/cm³
Te, keV
U, 10⁶ cm/s
Te
U
ρ
R, cm

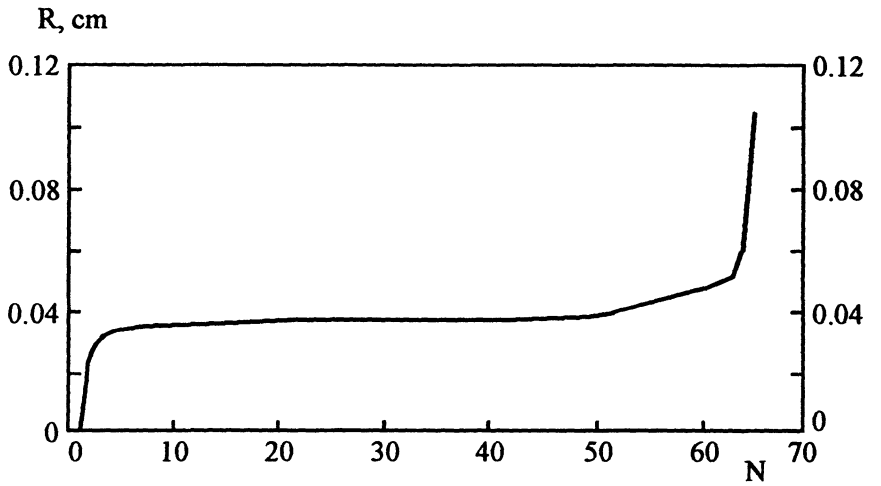

Fig. 7. Distributions of density ρ, electron temperature, and the plasma-motion velocity for $t = 1.5$ ns (corresponding to the flux peak): a) and b) in relation to the number of computational cells (total number of cells $N = 64$) drawn on different scales; c) in relation to the radius; d) plot illustrating the relationship between the cell number and the radius (for $t = 1.5$ ns).

of energy flux carried by electronic thermal conductance (flux E) and by radiation (flux R) over the target thickness. The magnitudes of fluxes are given in relation to the number of calculational cells for the problem as a whole (Fig. 9a) and on a more expanded scale (Fig. 9b). In order to obtain distributions over the radius, one should refer to Fig. 7d.

Figure 10 illustrates distributions of density, electron temperature, and the velocity of plasma over calculational cells for the instant of the laser-pulse end (3 ns). For the same point in time, Fig. 11a shows the fluxes of energy carried by electronic thermal conductances and radiation for the system as a whole, and Fig. 11b shows the same quantities on a more expanded scale.

5.3. Discussion of the Results of Calculation of Plasma Parameters

Figures 7a, 7b, 7c, and 10a show the spatial distributions of the density ρ, electron temperature T_e, and plasma velocity u for points in time of 1.5 and 3 ns. The distributions are typical for the problem under consideration; there are a region of low-density flying-off corona with a temperature amounting to about 1.2–1.5 keV (for $t = 1.5$ ns) and to about 0.2 keV (3 ns), a region of radiant heating with temperature of about 0.1 keV and $\rho \approx 0.1$ g/cm^3 (both for $t = 1.5$ and 3 ns), and a region of shock-compressed copper with density higher than nominal (≥ 10 g/cm^3) and temperature amounting to several electron volts. The zone of radiant heating is easily deduced from the distribution of radiation fluxes (Figs. 9a, 9b, 11a, and 11b). Absolute values of fluxes are not important for us; it is only significant that in this zone the radiation-related energy flux is many times larger than the flux of energy transported due to electronic thermal conductance. The velocity of the plasma expansion is 100–1000 km/s, whereas the velocity of the copper-shell motion in the region of radiant heating (with plasma density of 0.1 g/cm^3) is 50–100 km/s. For average value of laser-radiation flux equal to $2 \cdot 10^{14}$ W/cm^2 [t =1–2 ns], the corona temperature is adequately defined by formula (1) as

$$T = 0.4 \left(\frac{q}{10^{14}}\right)^{2/3} \left(\frac{1}{\lambda}\right)^{4/3} \text{[keV]}.$$

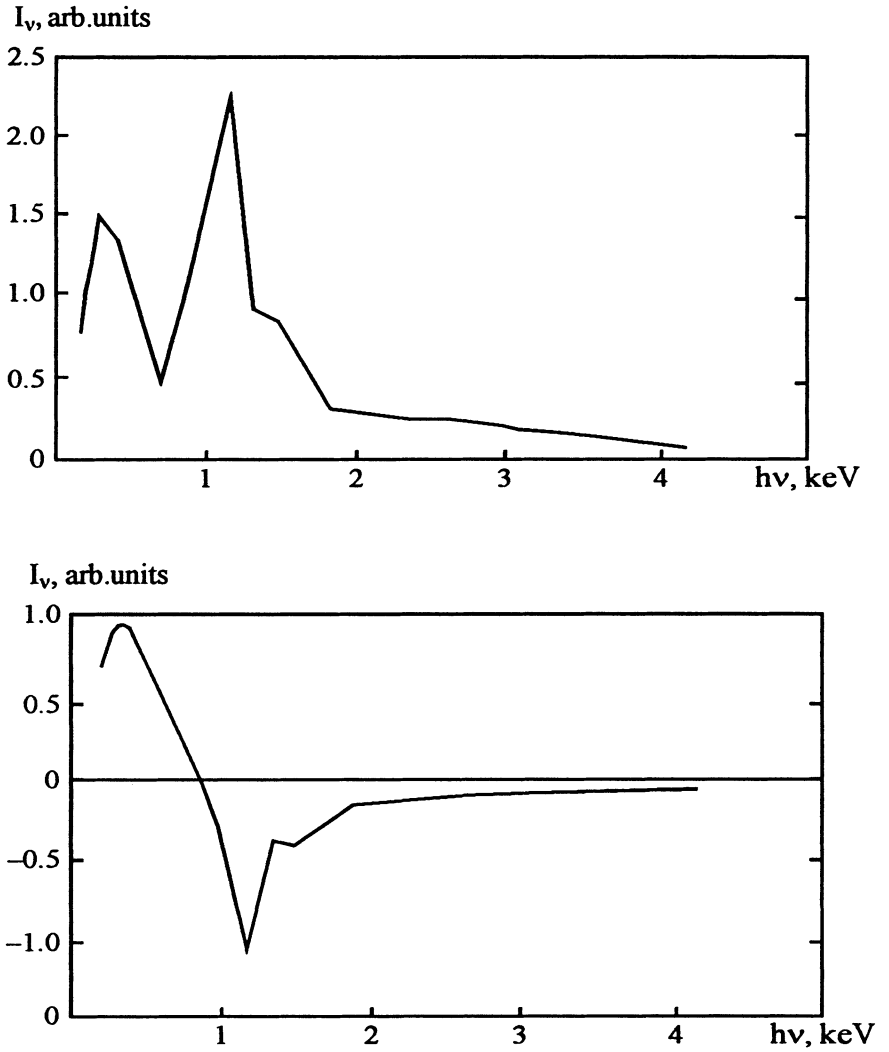

Fig. 8. Radiation flux I_ν as a function of the energy of quanta: a) at the plasma boundary (N = 64); b) at the boundary between the zone heated via electronic thermal conductance and the radiant-heating wave (N = 62).

The radiation spectra shown in Figs. 8a and 8b are understandably related to the distributions of density and temperature (Fig. 7a). The radiation flux is outwardly directed at the plasma boundary ($N = 64$). The soft component of radiation flux ($h\nu \leq 1$ keV) is outwardly directed and the hard component (corona emission with $h\nu \geq 1$ keV) is inwardly directed at the boundary between the wave fronts of electronic-conductance heating and radiant heating ($N = 62$).

It follows from these data that the soft component of the spectrum is defined largely by the wave front of heating due to electronic thermal conductance and partially by the main portion of the radiant-heating wave front. The hard component of the spectrum is completely defined by the corona emission. In Fig. 12, the calculated spectrum of radiation flux from copper shell (in this case, for $t = 1.5$ ns) is compared with the data reported in [13] for rhodium (see Fig. 4 in [13]). In the calculations, we take into account that (for $t = 1.5$ ns) 75 % of the incident laser radiation is emitted as x-rays and the intensity in a 4π-angle amounts to $0.55 \cdot 10^3$ J/(keV·ns) (taken as the intensity unit in Fig. 12). Experimental data were adopted from Fig. 4

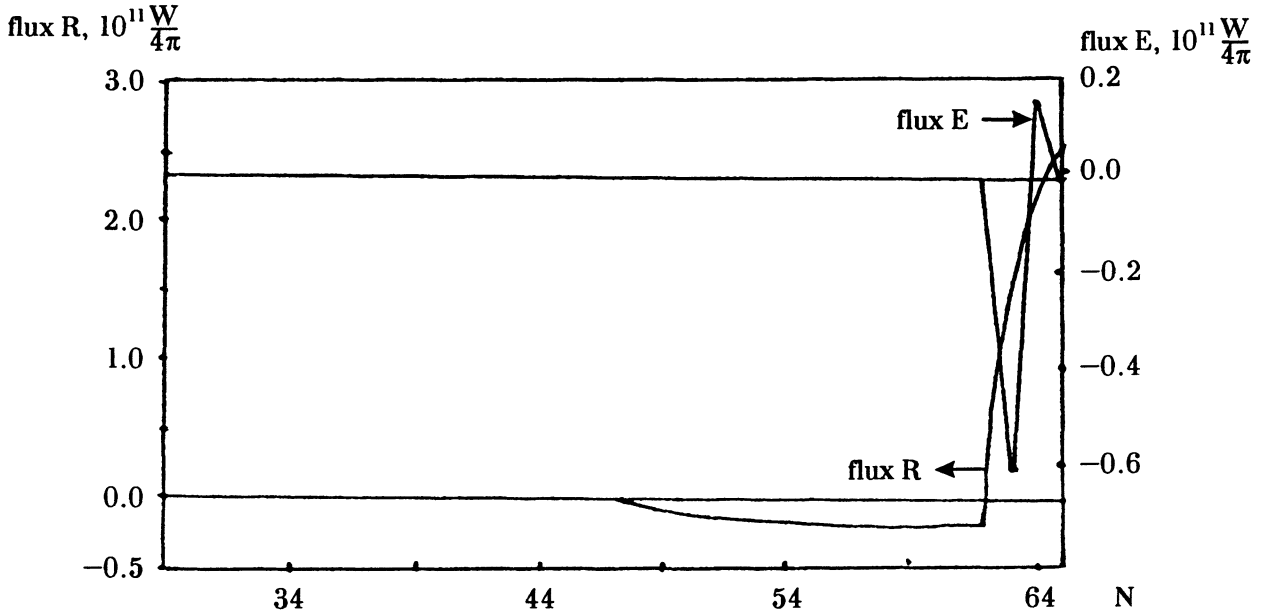

Fig. 9. The distribution with depth in the target for energy flux transported by electron-related thermal conductance (flux E) and by radiation (flux R).

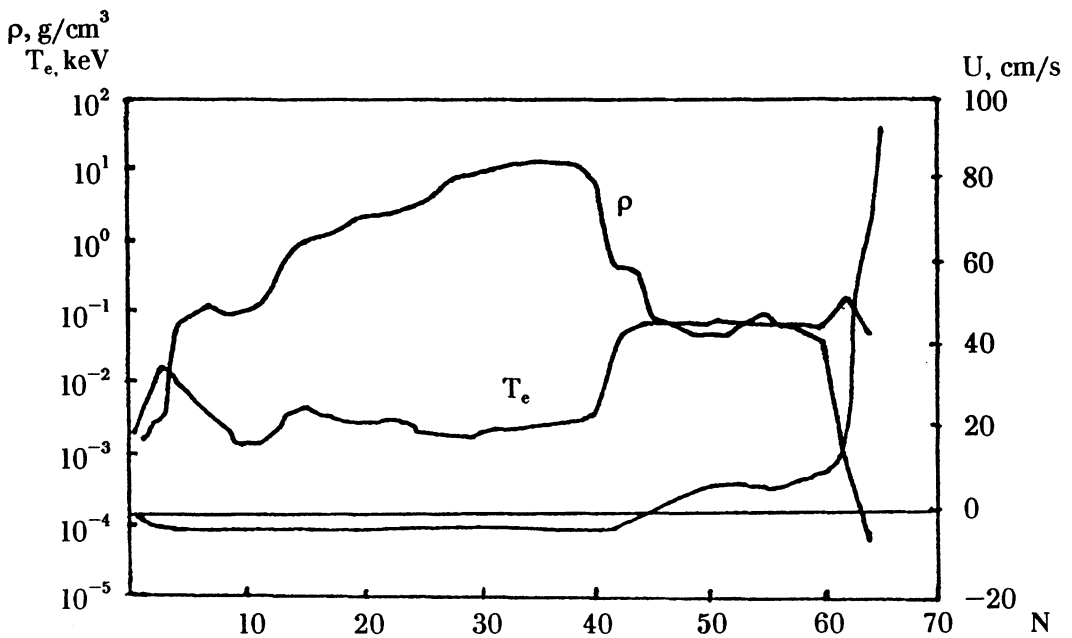

Fig. 10. Distributions of density, electron temperature, and velocity over computational cells for the time instant corresponding to the end of laser pulse ($t = 3$ ns).

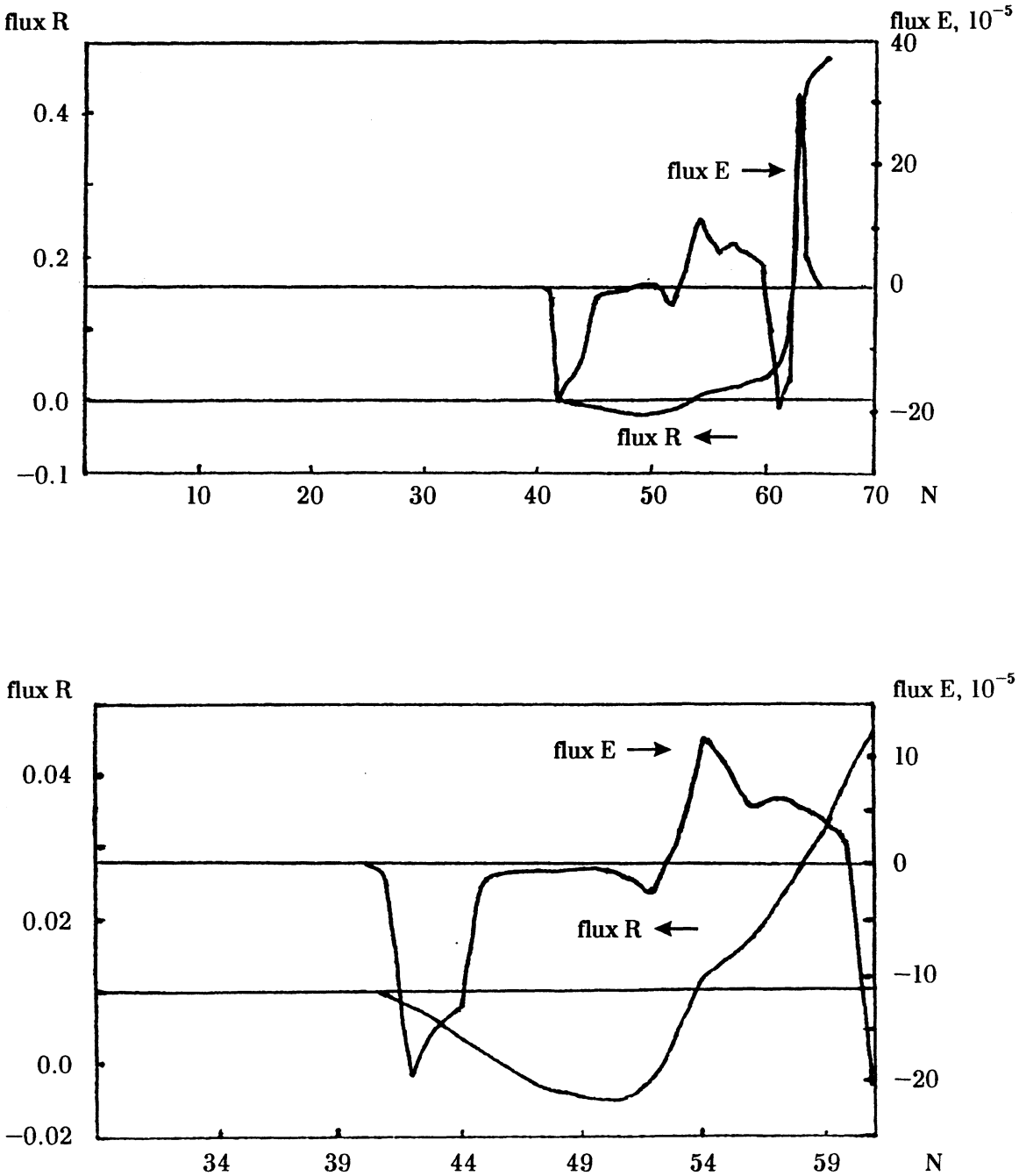

Fig. 11. Energy fluxes corresponding to electron-related (a) and radiant heat conduction (b) for the system as a whole.

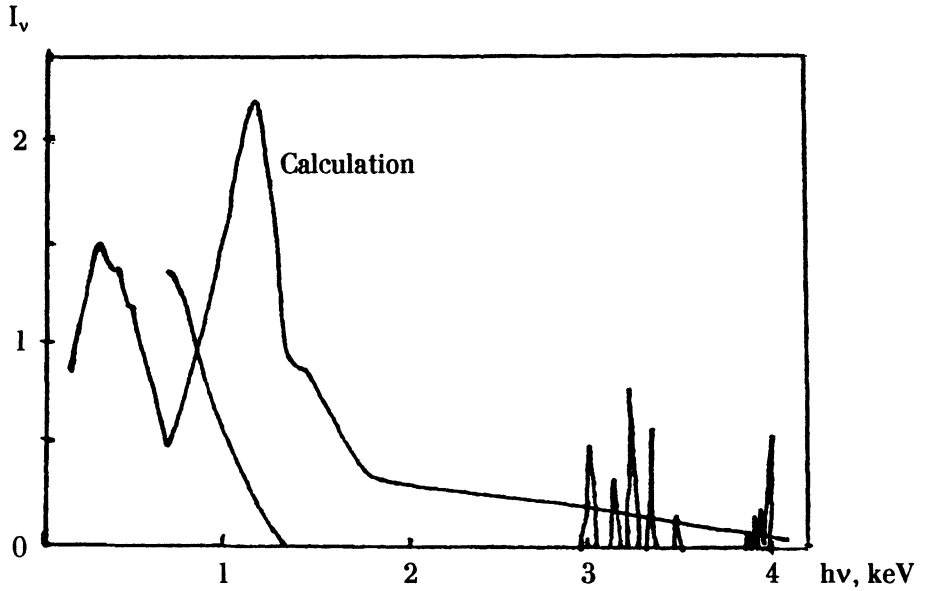

Fig. 12. Spectrum of radiation flux coming from a copper shell (as calculated for $t = 1.5$ ns) in comparison with the data reported for rhodium in [13].

in [13]. It is evident from Fig. 12 that the intensity and spectral distribution for copper and rhodium are nearly the same. In the case of copper, emission lines distinct in Figs. 5 and 6 appear in the spectrum in the ranges of 1–2 keV and 2–3 keV. In our calculations, these emission lines can be evaluated with the use of a special program which processes the results of calculations of the plasma temperature and density as obtained in the main code. However, it is unlikely that the intensities of these lines will be higher by an order of magnitude than the intensities of recombination radiation and bremsstrahlung. In this respect, the group constants account for a significant contribution of continuous component to the spectrum. This casts doubts on the experimental data [13] for rhodium. In Fig. 4 of [13], the radiation intensity varies by three orders of magnitude in the energy range of x-ray quanta of 1–3 keV, which hardly has any physical origin.

5.4. Evaluation of Parameters for a Laser-Plasma Cathode

The results of the above calculations verify the previously conjectured plasma parameters for the case of 3-kJ laser energy: the total number of electrons in the corona region is about $\sim 10^{19}$, the plasma expansion velocity is $8 \cdot 10^{-8}$ cm/s, and the plasma radius is 0.25 cm by the time of 3 ns. In a time of 10 ns, the plasma fills the volume with a radius of $8 \cdot 10^{7}$ [cm/s] $\times\, 10^{-8}$ [s] $= 0.8$ [cm].

If the charge of accelerated fast electrons is not compensated in the case of an accelerating voltage equal to about $\sim$50 keV and a cloud radius of about 1 cm, approximately $3 \cdot 10^{11}$ electrons (a fraction of $3 \cdot 10^{-8}$ of the total number of electrons within the corona) can be extracted from the cloud, which corresponds to the cloud's charge of about 150 esu. Even with allowance for a higher energy of accelerated electrons ($\sim$50 keV) as compared to the energy of plasma electrons ($\sim$1 keV), the intensity of emission of accelerated electrons is lower by a factor of 10^{-6} than that of plasma electrons. However, the former emission can be of higher energy and of higher degree of monochromaticity.

It is evident from examination of Figs. 7 and 10 that, as far as the conductance of the plasma is concerned,

the bottleneck here is bound to be the shock-compressed copper with density close to nominal and temperature amounting to several electron volts. If the electrical conductivity σ in this region is related to the plasma and is equal to about 10^{14} s^{-1}, a charge of $4 \cdot 10^3$ esu can be transported in 10 ns when the focal-spot diameter is $7.5 \cdot 10^{-2}$ cm and the electric-field strength is 1 cgs unit. This can compensate the space charge and make feasible the acceleration of about 10^{13} electrons. However, even this number of electrons is smaller than the total number of electrons in the plasma. The issue of what is the actual conductivity of substances under the conditions of interest is extremely complicated and calls for further investigation. Experiments with the current-induced rupture of wires provide certain information in this respect. Calculations related to shock-compressed region are, as a rule, unreliable because they are not based on adequate models. For example, it is easy to verify that in the case of copper with $\rho \simeq 10$ g/cm^3, $T = 1$ eV, and $Z = 1$ the Coulomb logarithm appearing in the expression for a conducting plasma is close to unity; under these conditions, theoretical models are typically inadequate.

Verification of the techniques of space-charge compensation for a plasma is desirable and promising; however, these efforts should indisputably be based on large-scale experiments because all the quantities of interest (the plasma surface, temperature, conductivity, and so on) depend on actual conditions and on the scale of experiment.

6. Monochromatic X-Ray Source Based on Ferroelectric Electron Emitter with Laser Mechanism of Polarization Reversal

6.1. The Methods of Producing the High-Energy Electron Beams with the Use of Ferroelectrics

Ferroelectrics with a controllable mechanism of spontaneous-polarization reversal are promising as sources of currents with high densities comparable to those considered in Sec. 1. The development of a ferroelectric-based source is a complicated challenge due to a wide variety of ferroelectric materials (including single crystals and ceramics) with a wide range of such important characteristics as spontaneous polarization P_s, coercive field E_c, and the Curie temperature T_C (the temperature corresponding to the transition to the ferroelectric phase).

(Pb,La)(Zr,Ti)O_3 (PLZT) ceramic can be chosen as one of these materials; this compound exhibits spontaneous polarization which is anomalously high for ferroelectrics and can be as high as 45 μC/cm^2.

Let us consider the mechanism of operation of such a source. A thin plate ($\Delta = 1$ mm) of PLZT with electrodes deposited on the surface is polarized perpendicularly to the electrodes. An electric charge arises at the electrodes, so that spontaneous polarization P_s tends to be compensated. The negatively charged electrode is provided with windows that expose the ferroelectric surface. A portion of the free charge compensating P_s resides directly on these windows. On the polarization-reversal in the ferroelectric, the surface charge is not held fixed by the ferroelectric's field, which can result in the emission of electrons with energies ranging from several to tens of kiloelectron volts [14]. In [15, 16], the 25-keV electrons were emitted during the phase transition in triglycine sulfate (TGS) crystals whose temperature was slowly elevated and passed through the Curie point. We expect that high-density electron beams can be formed in the processes related to fast polarization reversal and to the release of space charges during pulsed laser irradiation of a ferroelectric.

6.2. Qualitative Assessment of Emission of Electrons from the Ferroelectric Surface

In the ferroelectric changeover (reversal of the P_s vector), the charge at the exposed surface of ceramics is not retained any more by the field of the ferroelectric and can be removed. In the context of phenomenological theory, such a changeover is described in the following way [17]: Taking into account that the thermodynamic

potential of material (the Gibbs elastic energy) can be represented as a polynomial in the deviations from the initial state where $D_i = 0$, we may deduce the simplest model if we assume that the induction $D_i = D$ is aligned with one of the crystallographic axes (i.e., spontaneous polarization and electric field are directed along this direction), mechanical stresses are equal to zero, and the nonpolar phase is centrally symmetric. Each of these restrictions taken separately is not important; however, as a whole, they make it possible to define the free energy G_l in the simplest form as

$$G_l = \frac{\alpha}{2}D^2 + \frac{\gamma}{4}D^4 + \frac{\delta}{6}D^6 + \ldots, \tag{4}$$

where the energy is counted off from the value corresponding to nonpolar phase. In the simplest model suggested by Devonshire, it is assumed that

(i) the coefficients γ and δ are temperature-independent in relation to the first- and second-order transitions;

(ii) $\alpha = \beta(T - T_0)$ in the vicinity of the phase-transition temperature T_C, which corresponds to the experimentally observed behavior of ferroelectric materials (the Curie–Weiss law for dielectric constant);

(iii) the piezoeffect may be ignored;

(iv) the domain structure of ferroelectric may be discarded.

Assuming that $\gamma > 0$ (the second-order phase transition) we can restrict the thermodynamic-potential expansion to the first two terms:

$$G_l = -\frac{\beta}{2}(T_0 - T)D^2 + \frac{\gamma}{4}D^4. \tag{5}$$

Differentiantion of the Gibbs elastic energy with respect to D at constant temperature yields the following equation of state:

$$E = -\beta(T_0 - T)D + \gamma D^3. \tag{6}$$

Here, E is the electric field parallel to D. It is evident from examination of (6) that the behavior of $D(E)$ is different for $T > T_0$ and for $T < T_0$. At $T > T_0$, the material does not exhibit spontaneous polarization ($E = 0$, $D = 0$). With $T < T_0$ (in the case of a second-order transition T_0 coincides with T_C), a single value of E corresponds to two values of D, which are equal in modulus but have opposite sign (the branch with $dD < dE < 0$ is unstable); i.e., ferroelectric properties with the typical hysteresis loop are observed.

The spontaneous polarization is given by

$$P_s^2 = \left(\frac{D_0}{4\pi}\right)^2,$$

where D_0 is determined from the condition that $E(D_0) = 0$, so that

$$D_0 = \left[\frac{\beta(T_C - T)}{\gamma}\right]^{0/5}.$$

The coercive field is defined by the condition that $dE/dD = 0$; thus,

$$E_c = \frac{2}{\sqrt{27}} D_0\beta(T_C - T).$$

Expressing the coefficients β and γ in terms of the measured quantities E and P, we arrive at

$$\beta(T_C - T) = \frac{\sqrt{27}}{8\pi}\frac{E_C}{P_s}, \qquad \gamma = \frac{\sqrt{27}}{128\pi^3}\frac{E_C}{P_s^3}, \tag{7}$$

With $E = 2$ kV/mm and $P = 45$ μC/cm^2, we have

$$\beta(T_C - T) \approx 10^{-4}, \qquad \gamma \approx 3.4 \cdot 10^{-17}.$$

The dielectric constant for zero external field is written as

$$\varepsilon(0) = \left(\frac{dD}{dE}\right)_{E=0} = \frac{1}{2\beta(T - T_C)} = \frac{5 \cdot 10^3}{T - T_C}.$$

Taking into account that $T - T_C = 200$ K, we arrive at $\varepsilon(0) = 25$.

To a first approximation in E, we can use the following formula:

$$\varepsilon(E) = \frac{\varepsilon(0)}{1 \pm E/E_c}.$$

On the polarization reversal, the ceramic ferroelectric is bound to be heated. Furthermore, when the induction varies from 0 to $(2\text{–}3)^{-0.5}D_0$, the entropy decreases, which indicates that the work related to the polarization reversal should be done on the ferroelectric. The entropy is given by

$$S = -\left(\frac{\partial G}{\partial T}\right)_{D,X},$$

and, on the assumption that the coefficients β and γ are temperature-independent, we have $S = -0.5\beta D^2$.

When polarization is reversed in a ferroelectric, the decrease of entropy per unit volume amounts to

$$\Delta S = -\frac{4\beta^2(T_C - T)}{6\gamma},$$

and the work required to reverse the polarization can be evaluated as

$$A \sim -T\Delta S = \frac{4\beta^2}{6\gamma} T(T_C - T), \tag{8}$$

where T is the temperature of the ferroelectric sample, ΔS is the entropy variation, T_C is the Curie temperature, and β and γ are coefficients in the expansion of the Gibbs thermodynamic potential with the first two terms retained. Substituting the relevant numerical values into formula (8), we deduce that the specific work required to reverse the polarization in a PLZT ceramics amounts to about 30 J/cm^3. The heat released in a unit volume of ferroelectric is of the same order of magnitude. The behavior of the heat capacity can be evaluated as

$$C(D) = C_0 + \frac{\beta T}{2} \frac{d}{dT}(D_0 + \Delta D)^2,$$

where C_0 is the heat capacity of the nonpolar phase. Since $\Delta D = D - D_0$ is independent of temperature, we arrive at

$$C(D) = C_0 - \frac{\beta^2 T}{2\gamma} \left\{1 + \left[\frac{\gamma}{\beta(T_C - T)}\right]^{0.5} D - \left[\frac{\gamma}{\beta(T_C - T)}\right]^{0.5} D_0\right\}.$$

Assuming that temperature varies only slightly during the polarization reversal, we derive the following formula for the temperature variation:

$$\Delta T = -\beta \int_{1.73D}^{0} \frac{TD}{C(D)}\, dD. \tag{9}$$

In the discussion above, we considered a model of a second-order phase transition. The type of phase transition is difficult to identify experimentally owing to an appreciable temperature hysteresis. Therefore, in estimations it makes sense to analyze the processes within the framework of a simpler theory of the second-order phase transitions. The results are estimates and provide an adequate description of the behavior of thermodynamic quantities. Moreover, the question arises whether the thermodynamics is applicable at all to the phenomenon of fast polarization reversal in a ferroelectric. An appreciable insight can be gained with allowance for surface phenomena, defects, and domain structure in ferroectric, which can bring about a partial polarization reversal and incomplete hysteresis loops.

6.3. The Mechanisms of Fast Polarization Reversal

The time required for reversal of the vector P_s depends critically on temperature, the strength of the applied dc electric field, and a number of other factors [18]. Space-charge layers existing at the surface of a ferroelectric give rise to a strong electric field directed perpendicularly to the surface. If an electric field is applied to the crystal in a direction opposite to the direction of polarization, every antiparallel domain begins immediately to expand through the motion of the domain walls forward and sideways [19]. Rapid variation of P_s as a result of high-voltage pulses brings about large surface charges amounting to 0.1–1 C/m^2 and can initiate electron emission.

It should be expected that the highest surface-charge densities can be attained as a result of rapid reversal of the vector P_s combined with release of space charges under pulsed laser irradiation. Such a photoelectric effect will give rise to electron emission; consequently, ferroelectrics are promising materials for development of high-power electron emitters. Of particular interest is the reversal of the vector P_s in such a direction that electrons appear at the illuminated surface. To attain this, one should use electrodes which partially exposed surface. Rapid polarization reversal can be realized when the operating temperatures are close to the phase-transition point [20].

High-intensity electron emission caused by irradiation of a preliminary polarized ferroelectric sample by a high-power laser pulse (the wavelength $\lambda < 1$ μm) is feasible when simultaneous repolarization (related to pyroelectric effect) and space-charge release occur. Repolarization of the ferroelectric can be accomplished synchronously with laser irradiation with the use of high-voltage pulses.

Let us evaluate the external electric fields that are generated in a completely polarized system under condition that compensation of surface charges is prevented; we have

$$E = -\frac{P_s}{\varepsilon(0)\varepsilon_0}.$$

In the case of PLZT ceramics with $P_s = 45$ μC/cm^2 and $\varepsilon(0) = 25$, the external electric-field strength can be as high as 10^7 V/m. Such fields can be used to accelerate electrons, which was demonstrated in [21] when gradual phase transition in TGS crystals was studied.

We may assume that a laser with pulse duration of about 30 ps can be used to attain a current density as high as 10^4 A/cm^2; furthermore, the current density at an anode of about 1 mm in diameter can reach 10^7 A/cm^2, which is an order of magnitude higher than in the case of a diode with a laser-plasma cathode [9]. One may expect that optimization of pulse duration, wavelength, and energy of the heating laser, parameters and geometry of the crystal, and the parameters of the surrounding medium will make it possible to attain the predicted values of currents and electric fields; this, in turn, will make feasible an x-ray source with quantum energy in the range of 5–10 keV and spectral brightness higher than 10^{21} photons/(cm^2·s·sr·keV).

7. Summary and Conclusions

(I) Based on calculations of the plasma parameters for copper ($Z = 64$) and laser-radiation fluxes $q = 2.5 \cdot 10^{14}$ W/cm^2, we demonstrated that the soft component of x-ray radiation depends on the wave front of electron-related heating and partly on the major fraction of radiation-heating wave. The hard component of x-ray radiation is completely determined by the corona emission.

(II) It follows from calculations of the parameters of a laser-plasma diode for an energy of 3 kJ and accelerating voltage of ~50 keV that about 10^{19} electrons can be extracted from the plasma-generated cloud containing 10^{13} electrons. This signifies that the emission intensity for a laser-plasma diode amounts to $\sim 10^{-6}$ times the brightness of x-ray continuum of the plasma; however, this emission is harder and more monochromatic.

(III) The search for and verification of the mechanisms of the plasma space-charge compensation can be accomplished in a large-scale experiment because all the quantities of interest depend on actual experimental conditions and characteristic scales in the experiment.

(IV) The feasibility of accelerated-electron emitter based on a ferroelectric and controlled by laser radiation is demonstrated. Electron emission from the surface of the ferroelectric was quantitatively assessed. The power required for polarization reversal in the ferroelectric under laser-induced heating was determined.

(V) The mechanisms of rapid polarization reversal in ferroelectrics exposed to laser radiation were considered. It is demonstrated that electron-current densities as high as 10^7 A/cm^2 are attainable with the use of a laser with pulse duration of about 30 ps and a wavelength $\lambda \leq 1$ μm. This makes it possible to develop a point source that emits 5–10-keV x-ray quanta and has a spectral brightness as high as 10^{21} photons/(cm^2·s·sr·keV).

Acknowledgments

This work was supported by the Russian Foundation for Basic Research under Projects Nos. 95-02-18750, 96-02-04264, and 97-02-17852 and by INTAS under Grant No. 94-1937.

References

1. M. H. Key, R. G. Evans, and D. J. Nicholas, "Study of ablatively imploded spherical shells," Preprint No. NRL-78-020 of the Rutherford Laboratory (1978).
2. M. H. Key, P. T. Rumsby, R. C. Evans, et al., *Phys. Rev. Lett.*, **45**, 1801 (1980).
3. G. Bayer, D. Billon, M. Decroisette, et al., in: H. Schwarz, H. Hora, M. Lubin, and B. A. Yaakobi (Eds.), *Laser Interaction and Related Plasma Phenomena*, Plenum Press, New York (1981), Vol. 5, p. 596.
4. C. Yamanaka, S. Nakai, Y. Kato, et al., in: H. Schwarz, H. Hora, M. Lubin, and B. A. Yaakobi (Eds.), *Laser Interaction and Related Plasma Phenomena*, Plenum Press, New York (1981), Vol. 5, p. 541.
5. D. T. Attwood, *IEEE J. Quantum Electron.*, **QE-14**, 909 (1978).
6. D. T. Attwood, N. M. Ceglio, E. M. Campbell, et al., in: H. Schwarz, H. Hora, M. Lubin, and B. A. Yaakobi (Eds.), *Laser Interaction and Related Plasma Phenomena*, Plenum Press, New York (1981), Vol. 5, p. 432.
7. D. L. Matthews, "Laser-produced x-ray sources for use in x-ray radiography," in: 1981 Laser Program Annual Report, LLNL Report NUCRL-50021-81 (1982).
8. H. Nishimura, H. Niki, N. Miyanaga, et al., *Rev. Sci. Instrum.*, **56**, 1128 (1985).
9. M. V. Dmitriev, Yu. A. Zakharenkov, and A. S. Shikanov, "Emission of K lines from a vacuum diode with laser-plasma cathode," Preprint No. 91 of the P. N. Lebedev Physical Institute, Moscow (1989).
10. O. V. Bogdankevich, V. Yu. Sudzilovskii, and A. A. Lozhnikov, *Zh. Tekh. Fiz.*, **35**, 2052 (1965).

11. I. B. Borovskii, *Physical Foundations of X-Ray Spectrum Studies* [in Russian], Nauka, Moscow (1956).
12. I. S. Tilinin, *Poverkhnost*, No. 8, 5 (1988).
13. B. A. Remington, S. W. Haan, S. G. Glendinning, et al., *Phys. Fluids* B, **4**, 967 (1992).
14. I. S. Rez, G. I. Rozenman, Yu. L. Chepelev, et al., *Pis'ma Zh. Tekh. Fiz.*, **5**, 1352 (1979).
15. H. Gundel, H. Riege, and E. J. N. Wilson, *Nucl. Instrum. Meth. Phys. Res.* A, **280**, 1 (1989).
16. G. I. Rozenman, V. I. Pechorskii, Yu. L. Chepelev, et al., *Phys. Status Solidi B*, **120**, 667 (1983).
17. M. E. Lines and A. M. Glass, *Principles and Applications of Ferroelectrics and Related Materials*, Clarendon Press, Oxford (1977).
18. W. J. Merz, *J. Appl. Phys.*, **27**, 938 (1956); *Phys. Rev.*, **88**, 421 (1952); *Phys. Rev.*, **95**, 690 (1954).
19. V. Janovec, *Czech. J. Phys.*, **9**, 468 (1959).
20. J. Handerek and K. Roleder, *Ferroelectrics*, **76**, 159 (1987).
21. Yu. V. Afanas'ev, E. G. Gamalii, N. N. Demchenko, and V. B. Rozanov, "Physical relationships in the 'corona' of spherical laser targets," *Proceedings of the P. N. Lebedev Physical Institute* [in Russian], Nauka, Moscow (1982), Vol. 134, p. 42.